Chapter 3: Finite Element Analysis of the nano-RDMA Geometry

3.1. Introduction

Measurements of the particle size distribution of aerosol nanoparticles have enabled new fundamental information about the atmosphere,[1] *in situ* optimization of nanoparticle production,[2] and controlled investigations of aerosol dynamics.[3] At the heart of these measurements is the differential mobility analyzer (DMA). A DMA classifies charged aerosol particles according to their mobility (Z_P) in an electric field (E) between two electrodes (spaced a distance b apart). Particles enter the classifying region where the electric field is present and traverse a particle-free sheath flow (Q_{sh}). Particles with a certain mobility will exit through the opposite electrode after a fixed distance in the electric field. The device specifics (i.e., electrode spacing, sheath flow rate, geometry, and classifying region length) determine the voltage (V) required to obtain the requisite electric field to transmit particles of a particular range of mobilities through the device. The relative range of mobility distributions transmitted determines the instrument resolution. Resolution along with fraction transmitted and size range are the important characteristics of device performance.

A recent trend of aerosol research has been to develop tools capable of measuring particle size with atomic dimensions.[*4-7*] The major theoretical limitation on device performance for small particles is diffusion.[*8*] Diffusion spatially broadens the particle

distribution within the DMA, resulting in a broader range of voltages over which particles of a fixed single mobility are transmitted. Diffusion simultaneously limits transmission, as the spatial broadening of the distribution results in losses to the walls of the device.

Improving resolution and transmission is typically accomplished through reducing residence time and, therefore, spatial broadening of the particle distribution in the device. Residence time can be decreased either through increasing the sheath flow rate (Q_{sh}) or decreasing the spacing between the aerosol entrance and sample exit. The sheath flow rate can be increased up to the point where turbulence is induced, and the spacing between entrance and exit can be decreased only to a certain extent.

It has been shown that an optimum exists in the classifying column length for the cylindrical DMA (cDMA) geometry that consists of two coaxial cylinders with R_2 and R_1. The condition that maximizes resolution is when the sizing column length is equal to the electrode spacing (i.e., $l = R_2 - R_1$). The optimum dimensions are not as clear for the Radial DMA (RDMA). The RDMA consists of parallel disk electrodes with the aerosol entering at R_2 and exiting through a hole in the center of the opposite electrode with a radius R_1.

The theoretical guidelines for optimum performance are straightforward in appearance, but the actual device performance is usually less than theoretically predicted. The most significant limit on achieved resolution experimentally is usually attributed to electrode alignment for the cDMA and Winklmayr DMAs, as axial asymmetry has a significant impact on resolution. Often the impact is significant enough to warrant extreme care in alignment in order to achieve absolute best tolerances. The electrode

alignment in the RDMA also impacted the achieved resolution in the original RDMA, but this inefficiency has been limited in the design of the nano-RDMA.

The device transmission also improves with decreased residence time. The transmission through the classifying region is often secondary in importance as other areas impact transmission through losses due either to electrophoresis or to diffusion. These areas are often three dimensional in nature and therefore will not be treated due to memory limitations. For the purposes of this section, only transmission in the sizing region was considered.

Perfect agreement is not expected between theoretical and experimental results, but a few assumptions could be responsible for some of the disparity. The major simplifications in the theoretical analysis are the assumptions of a uniform electric field, a parabolic or plug flow profile, and a dirac delta function for the aerosol input location. The assumption of a dirac delta distribution at the inlet is actually quite good. The initial spatial distribution of the particles is quite finite provided that the gap of the aerosol inlet is set properly. Too wide of a gap would have the same effect as diffusion.

The assumption of uniform electric field is more problematic. The best electrode alignment will not ensure an electric field that is uniform throughout the device. The electric field in the area near the aerosol inlet and outlet is not perfectly axial, as the electrodes are not solid. The electrodes must permit particle transmission, resulting in some degree of field penetration or distortion in these areas. These non-uniformities should remain azimuthally symmetric, but could potentially impact the device performance.

The assumed flow profiles and field are not entirely correct for either the radial DMA (RDMA) or cylindrical DMA (cDMA) configuration. The flow field separates in the center of the RDMA, a clear deviation from the ideal flow profiles. The flow profile in the cylindrical DMA is disrupted by the introduction of the aerosol stream and the removal of the sample stream. These effects should be more substantial for DMAs where the aerosol inlet and outlet are a significant fraction of the device size than they are for the designs used to measure larger particles.

These assumptions have enabled theoretical analysis to provide guidelines for DMA design, but the actual impact of each assumption requires a computational approach to evaluate. For the purposes of this paper, we will present simulation results of the recently developed nano-RDMA.[*9*] The nano-RDMA was developed to measure nanoparticle size in the 1 to 12.5 nm range with high resolution and therefore the classifying region is small. Any non-idealities in design are magnified as they comprise a significant portion of the classifying region. For most DMA designs, lack of axial symmetry or concentricity is usually a major factor, but the nano-RDMA was designed to ensure a high degree of concentricity. While manufacturing perfection was not achieved with the nano-RDMA, improvements in resolution should also be achievable through design improvements.

In a previous report, finite element modeling of the aerosol behavior inside a mobility analyzer provided a clearer picture as to the deficiencies of the device operation.[*10-11*] Altering the device construction resulted in improved performance. In this report, we will present geometry modifications of the nano-RDMA that were simulated to determine the effect on resolution and transmission. We will explore how

simulated results deviated from theoretical assumptions. Finally, we will discuss recommendations for improvements.

3.2. Theoretical Considerations

The internal structure of the nano-RDMA was modeled assuming a two-dimensional axisymmetric geometry—a full-scale three-dimensional model was computationally prohibitive. Consequently, the results fail to capture some of the dynamics of the racetrack region, the aerosol inlet extension, the sheath gas distributor porous material, and the three-dimensional aspects of the mesh on the excess outlet. The racetrack region is included in the model in an axisymmetric manner so that particle deposition as the aerosol passes through the knife edge region is captured qualitatively. A separate analysis will be given for the aerosol inlet extension.

A MatLab script was used to generate the model geometry to be tested to permit facile testing of numerous parameters of the nano-RDMA. The standard model is shown in figure 3.1. The script enabled multiple permutations to the standard geometry, including the following parameters: (1) the knife edge gap size (parameter *a*), (2) the sizing column size (parameter *b*), and (3) the aerosol outlet size (parameter *c*). Additional simulations investigated the effect of the mesh on the excess outlet and the effect of aerosol flow rate. A majority of the simulation used the aerosol and sheath flow rates of 0.6 and 10 standard liters per minute (SLM) used in calibrating the nano-RDMA. The more common flow rates of 1 and 10 SLM (aerosol and sheath respectively) were simulated as well. Finally, a comparison is made between the nano-RDMA and the original RDMA.[*12*] The angle of convergence of the bottom plate was also simulated

but the results will not be presented here. Converging DMAs are known to result in lower resolution and this result was confirmed in the simulations.

For each set of parameters, the fraction transmitted (i.e., flux exiting the sample outlet divided by flux entering the aerosol inlet) was recorded for particles with integer mobility diameters in the range of one to ten nanometers. For each diameter, the geometry was simulated for a range of voltages around the ideal transmission voltage for the particle mobility diameter for the standard geometry. The step size for voltage variation was 0.005 of the ideal voltage.

The geometry was constructed and then loaded into a second MatLab script to be analyzed. The same script could be used for most of the different simulations.[*13*] The script allowed COMSOL to generate a standard mesh for the geometry that is refined using the standard method twice to generate a finer mesh followed by two further refinements of the mesh in sizing region of the device. Fewer refinements in the mesh resulted in poor performance of the model wherein the concentration profile did not match expected behavior or the mesh did not have sufficient density to ensure convergence.

The simulations required three modules to be solved to determine transmission for a given geometry: electrostatics, incompressible Navier-Stokes, and electrokinetic flow. The modules were solved sequentially rather than simultaneously, as the later is very memory intensive. The electrostatics module was solved first and then the incompressible Navier-Stokes and finally the electrokinetic flow. The incompressible Navier-Stokes module was only solved once for each geometry model since changing particle size and applied voltage did not affect the flow field. Rather than solving the

electrostatic module multiple times for each voltage and geometry, the electrostatic module was solved with the voltage scaled between zero and unity. The magnitude of the voltage was accounted for in the electrokinetic module through multiplying the particle mobility by the voltage. The electrokinetic module was solved repeatedly for each voltage, particle size, and geometry.

The transmission data were compiled, and a MatLab script was used to compute the calibration factor for the geometry, the transmission, and the resolution. The calibration factor was determined from fitting the transmission data as a function of voltage for each particle size to a lognormal distribution. From the product of the particle mobility and the geometric mean, the calibration factor was determined. The transmission and resolution were found using a separate fitting function that used the Stolzenburg transmission function and the non-linear fitting program *nlinfit* of MatLab. The program fit the transmission data using the following equation:

$$f\left(Z_P\right)=\frac{\Gamma_{out}}{\Gamma_{in}}=\eta\left(Z_P^*\right)\Omega_{Stolzenburg}\left(Z_P,Z_P^*,\beta,\delta=0,\sigma_{Stolzenburg}\right), \qquad 3.1$$

where $f(Z_P)$ is the ratio of the flux leaving the sampled outlet (Γ_{out}) to the flux entering the aerosol inlet (Γ_{in}), $\eta(Z_P^*)$ is the mobility dependent transmission efficiency, Z_P^* is the ideal mobility of a particular particle size, $\Omega_{Stolzenburg}$ is the Stolzenburg transfer function, β is the ratio of the aerosol to sheath flow rate (Q_a / Q_{sh}), δ is a parameter accounting for unbalanced flows (here it is 0), and $\sigma_{Stolzenburg}$ is the Stolzenburg broadening coefficient. The fitting routine solved for $\eta(Z_P^*)$ and $\sigma_{Stolzenburg}$ for each particle size, and subsequently converted $\sigma_{Stolzenburg}$ to a resolution.

3.3. Results and Discussion

3.3.1. Electrostatics

The solved electrostatic module for the standard geometry is shown in figure 3.2. The electric field lines were perpendicular to the z-axis for the most part with the exception of three locations where distortions from the uniform electric field lines are found. The first location is near the sample outlet where the electric field lines point toward the bottom plate. This distortion would cause charged particles to migrate in the direction of the arrow. Unlike the excess outlet, the sample outlet was not covered with a mesh, as this would impact particle transmission. The second distortion location was near the sheath gas inlet. As the particles were not introduced into this region, the electric field was not as important here as it is in other places. The final field distortion location was near the knife edge inlet, which is shown in greater detail in figure 3.3. The electric field was reduced in strength and is non-uniform across this region, providing a distribution of electric fields that particles experience upon entering the sizing portion of the device. The arrow indicating direction of the electric field on the top of the knife edge actually pointed upward. This would result in a favorable narrowing of the distribution as it emerges from this region that would improve the assumption of a dirac delta distribution of particles entering the classifying region.

The permutation from the standard geometry that caused the greatest divergence of the electric field was the removal of the mesh on the excess outlet. Removing the mesh on the excess outlet caused the electric field to be distorted in the excess outlet region in addition to the distortions in the electric field present with the mesh, as shown in figure 3.4. Also, the average magnitude of the electric field was less without the mesh

than with the mesh. A higher applied voltage was necessary to create the same magnitude of electric field.

3.3.2. Incompressible Navier-Stokes

The solution to the incompressible Navier-Stokes for the standard geometry is presented in figure 3.5. The streamlines were inclined relative to the electrode and not parallel as the parabolic and plug flow profiles assume. This should not affect particle transmission or resolution as the particles must traverse the same total amount of sheath gas to reach the streamlines exiting as the sampled flow. This solution changed only in minor ways with all geometry permutations. One unexpected behavior was that the separation streamline occurred closer to the middle of the gap than would be expected based on the ratio of the flow rates of 0.6 SLM sampled flow and 10 SLM excess flow, but no apparent recirculation zone was found at the separation streamline. The second insight obtained was that the high flow rate in the excess outlet results in a correspondingly high Reynolds number in this region and presents the main limitation to increasing the sheath flow rate. The diameter could be expanded here to permit operation with a higher sheath flow rate.

3.3.3. Electrokinetic Flow

The solution to the electrokinetic flow module for the standard geometry is presented in figure 3.6 with the applied voltage set as the theoretical voltage. The particles enter through the knife edge gap and remain narrowly distributed in space until they reach the area below the mesh. The particle stream in this area distributed more broadly in space with a fraction of the particles exiting with the excess outlet flow, and

the remaining particles exit with the sampled outlet flow. If this solution was overlaid on the incompressible Navier-Stokes solution, the region where this separation occurred does not overlap with the location where the separation of flow stream lines do. The electric field must force the particles through the location where the streamlines separate. If an actual recirculation zone did appear in this region,[*14*] the electric field should prevent any charged particles from accumulating.

Without the mesh, the particle trajectories change substantially for the same applied voltage, as shown in figure 3.7. The average field strength was reduced to the point where the entire particle stream exited the device with the excess flow. A higher applied voltage was required to transmit particles to the sampled outlet.

3.3.4. Calibration Factor

The calibration factor was determined for the different geometry permutations modeled. It was found to be 110.2 cm^2/s for the standard geometry with the mesh in place, whereas it was 131.4 cm^2/s without the mesh. The experimentally determined value of the calibration factor (125.6 cm^2/s)[*9*] is between these two limits. This suggests that the mesh does not ensure electric field uniformity across the entire outlet. It is plausible that the porous nature of the mesh diminished the effective field in the center of the device introducing electric field non-uniformities. The magnitude of the electric field on the mesh could be altered independently to simulate the porous nature of the mesh as it was a separate boundary in the model. Using a value of between 0.85 and 0.90V on the mesh boundary reproduced approximately the experimentally observed calibration factor.

The other parameters that affect the calibration factor were the gap between plates (*b*), the aerosol outlet gap (*c*), and the aerosol inlet gap (*a*). Smaller gaps between the

electrodes decreased the calibration factor, as shown in figure. 3.8. The decreased gap caused the flow to accelerate, but simultaneously increased the electric field and decreased the axial distance necessary to travel to be transmitted to the sampled flow. The aerosol inlet gap changed the effective electrode spacing and therefore affected the calibration factor in a similar manner, as shown in figure 3.9.

The aerosol outlet gap determined the length of the classifying column. Smaller outlet gaps corresponded to a longer classifying region and a more uniform electric field, resulting in a smaller calibration factor, which was consistent with theoretical expectations. The calibration factor determined for changes in the aerosol flow rate (Q_a). changed only in a minor way (less than 1%) and this was reflected in the theoretical equation for transmission that omitted this variable.

3.3.5. Resolution

The transmission data for the different particle sizes was well fit using the Stolzenburg transfer function to obtain the resolution of the standard geometry, which is shown in figure 3.10. The resolution rose sharply and leveled off at a value of approximately 15. This was lower than expected since the theoretical limit is 16.7, a value based on the ratio of the sheath to aerosol flow rate.[*8*] The possible causes for this behavior were the electric field distortions near the aerosol inlet and outlet, and the spatial broadening in the region near the mesh. Examining the electrokinetic module, the spatial broadening of the distribution before the region near the mesh was minimal and therefore was less likely responsible for the deviation. However, the spatial broadening near the mesh was more significant and was a possible cause of the lower-than-expected resolution.

The resolution without the mesh was lower than the resolution with the mesh even though the voltage used to classify particles of the same mobility was higher without the mesh. The solution without the mesh has the same distortions near the aerosol inlet as the one with the mesh. Yet, the one without the mesh has a greater degree of distortion in the region near the mesh that could be responsible for the difference. These results suggested that the field distortions can affect resolution even when axis-symmetric.

The second important parameter simulated was the separation between the electrodes, the results of which are shown in figure 3.11. The electrode separation (b) that maximized resolution was 7.5 mm. The simulations indicated that an optimum existed for the RDMA when the aerosol inlet radius (R_2) is equal to the electrode gap (b), suggesting that the aerosol outlet gap (R_1) did not impact the resolution. Simulations that varied the aerosol outlet gap (c) showed that the resolution is only affected in a minor way by this parameter, as shown in figure 3.12. Reducing the electrode spacing to 7.5 mm will limit the maximum operating voltage of the nano-RDMA to 7.5 kV. The impact of such a change on maximum measurable particle size would need to be determined experimentally. This improvement did increase the resolution to about 15.7 but still not to the theoretical limit.

The aerosol inlet gap did have a small impact on resolution, as shown in figure 3.13. Decreasing the gap spatially restricted the particles, which improves the resolution slightly. Simulating a geometry with the optimal electrode spacing (b = 7.5 mm) and the optimal inlet gap did not lead to a further improvement in resolution.

The inability to achieve the maximum resolution indicated a minor inherent inefficiency in the RDMA design. Examining the electrokinetic result at the voltage

corresponding to the maximum transmission showed an incomplete separation, see figure 3.14. A portion of the aerosol exited with the excess flow, indicating that at maximum transmission the voltage is not sufficient to drive all of the particles into the sampled outlet flow. The cause could be the non-uniform electric field in the aerosol outlet region. The electric field directed the particles toward the bottom plate, expanding the aerosol over a broader region. Using a higher voltage than optimum would improve the separation, but would simultaneously force particles to deposit on the bottom plate. The net result of the incomplete separation was a broadening of the measured distribution and a maximum resolution that was lower than theoretically achievable.

A more uniform electric field could be generated for the purposes of these simulations using a flat internal boundary across the aerosol sampled outlet. The model could not be solved with this change due to memory limits, as the second internal boundary created a high density of mesh points.

Overall, the resolution of the nano-RDMA is still considerably better than the resolution of the RDMA for the 1 to 10 nm size range, as shown in figure 3.15. The maximum resolution achieved is higher for the nano-RDMA, as well. The lower maximum resolution for the RDMA is most likely a result of the spacing between the inlet and outlet (R_2) being more than the electrode gap (b). The figure includes the resolution for the higher aerosol flow rate of 1 SLM for the nano-RDMA and RDMA. The maximum resolution is again lower than the theoretical value for most likely the same reasons as described before.

3.4. Summary

The resolution of the current nano-RDMA can be improved through decreasing the electrode spacing (b) to a value of 7.5 mm. The optimum condition for the RDMA geometry is therefore when the inlet radius (R_2) equals the electrode spacing (b). Modifying the electrode gap maximized the resolution, but did not quite achieve the theoretical resolution most likely due to a non-uniformity in the electric field. The simulation results indicate that the assumptions of parabolic/plug flow profile and dirac delta spatial distribution at the inlet were approximations but did not impact the resolution. The assumption of uniform electric does impact the resolution as the non-uniform electric field in the aerosol outlet region spatially broadens the distribution.

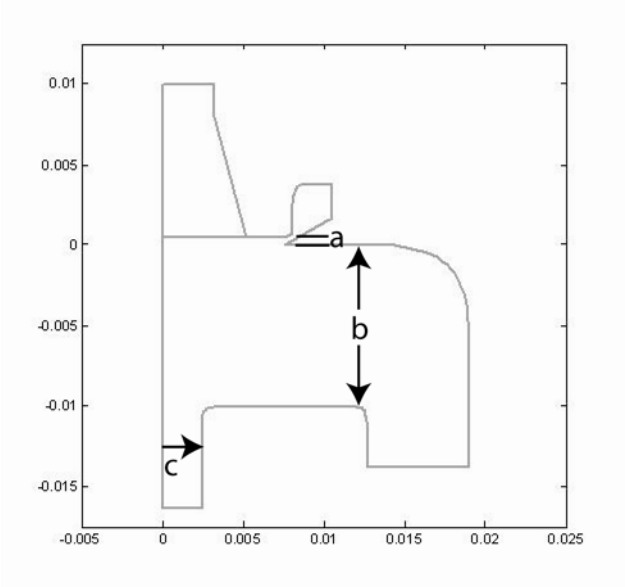

Figure 3.1. Outline of the Axis-Symmetric Model.

Outline of the axis-symmetric two-dimensional model used to calculate the resolution of the nano-RDMA. The aerosol inlet gap (a), the electrode spacing (b), and the aerosol outlet gap (c) are labeled accordingly.

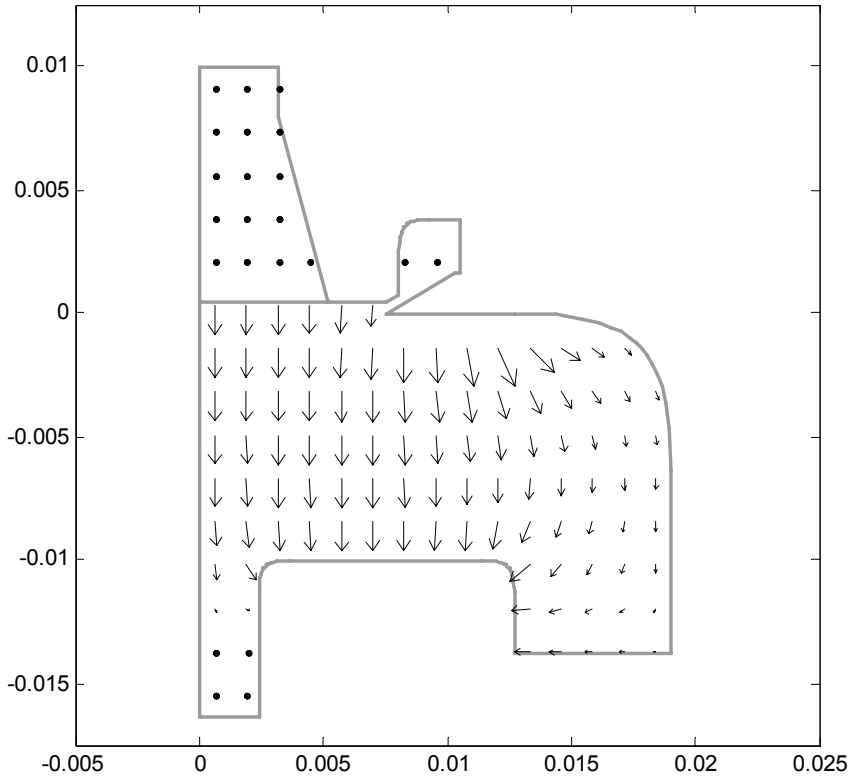

Figure 3.2. Electrostatics Solution.

Solution of the electrostatics module for the standard nano-RDMA geometry.

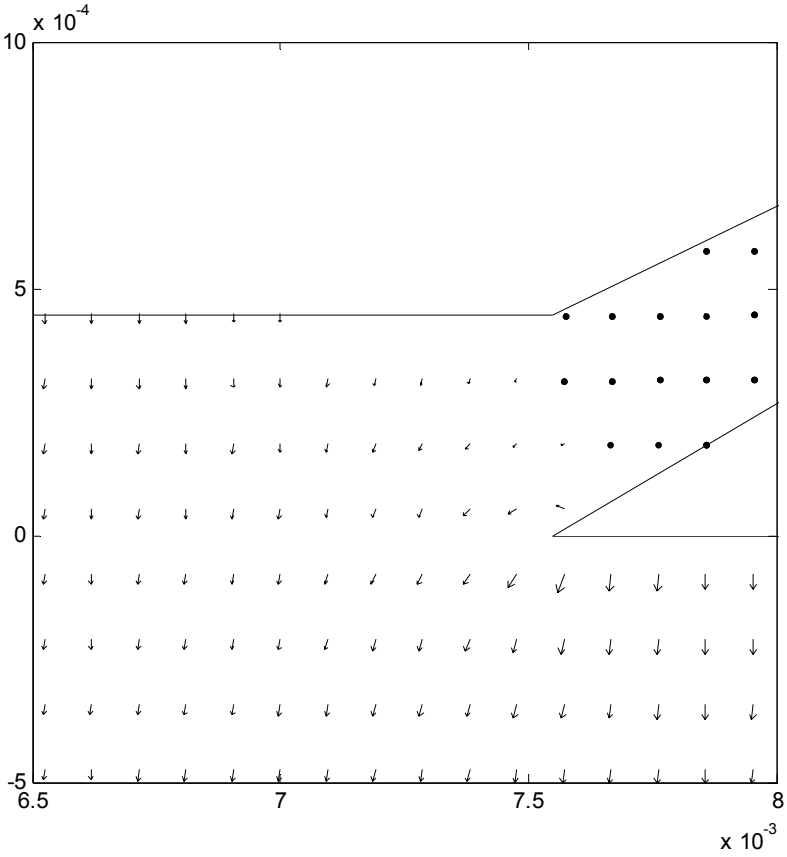

Figure 3.3. Inset of Aerosol Inlet Region.

Inset of the aerosol inlet region demonstrating the direction of the electric field.

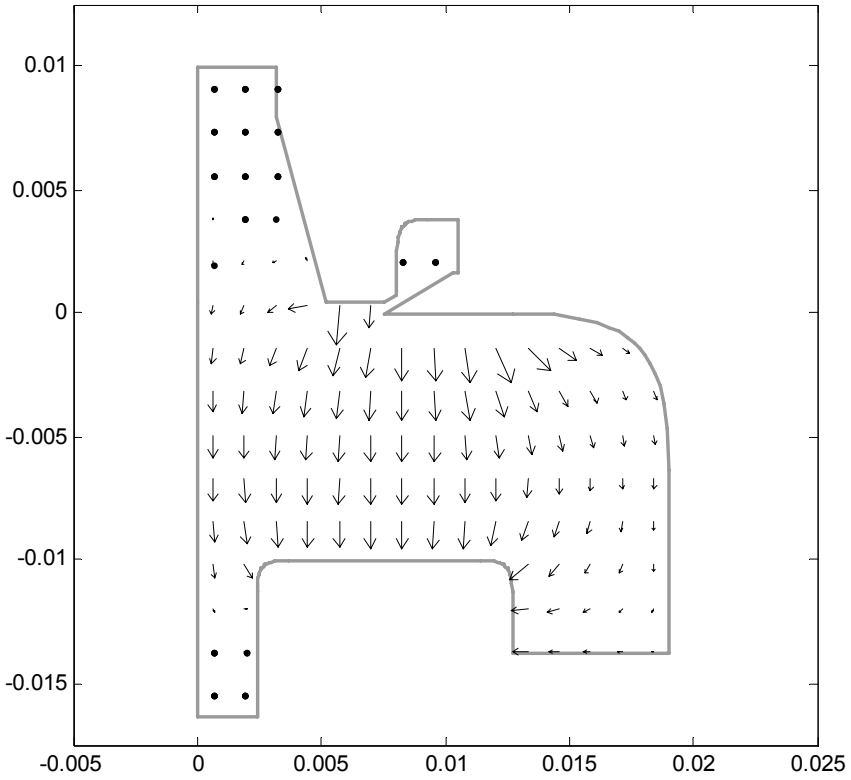

Figure 3.4. Electrostatics Solution without Mesh.

Solution to electrostatics module for the standard geometry without the mesh on the excess outlet.

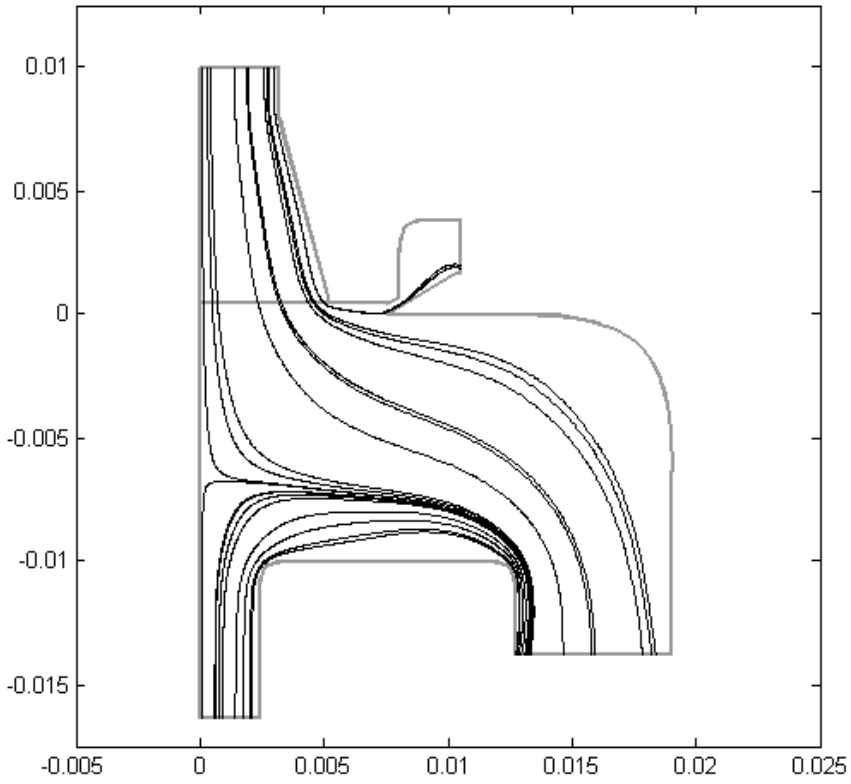

Figure 3.5. Navier-Stokes Solution.

Solution to the incompressible Navier-Stokes module for the standard nano-RDMA geometry. The flow rates are balanced with an aerosol and sheath flow rate of 0.6 and 10 SLM, respectively.

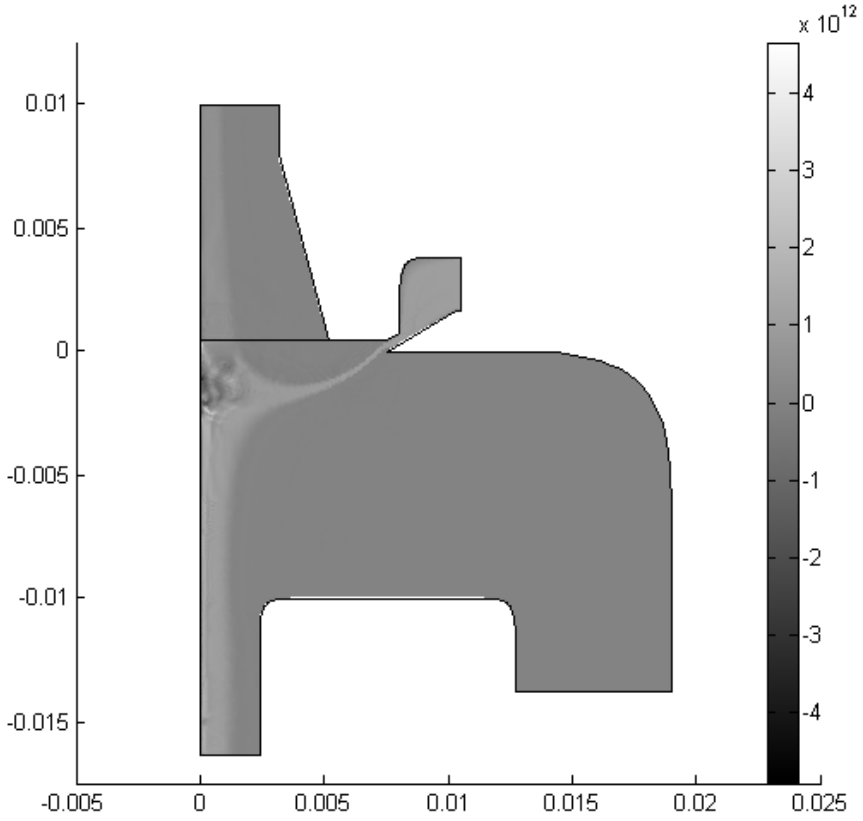

Figure 3.6. Electrokinetic Flow Solution.

Solution to electrokinetic flow module for the standard nano-RDMA geometry for particles with a 10 nm mobility diameter. The applied voltage is the theoretical voltage necessary to transmit 10 nm particles.

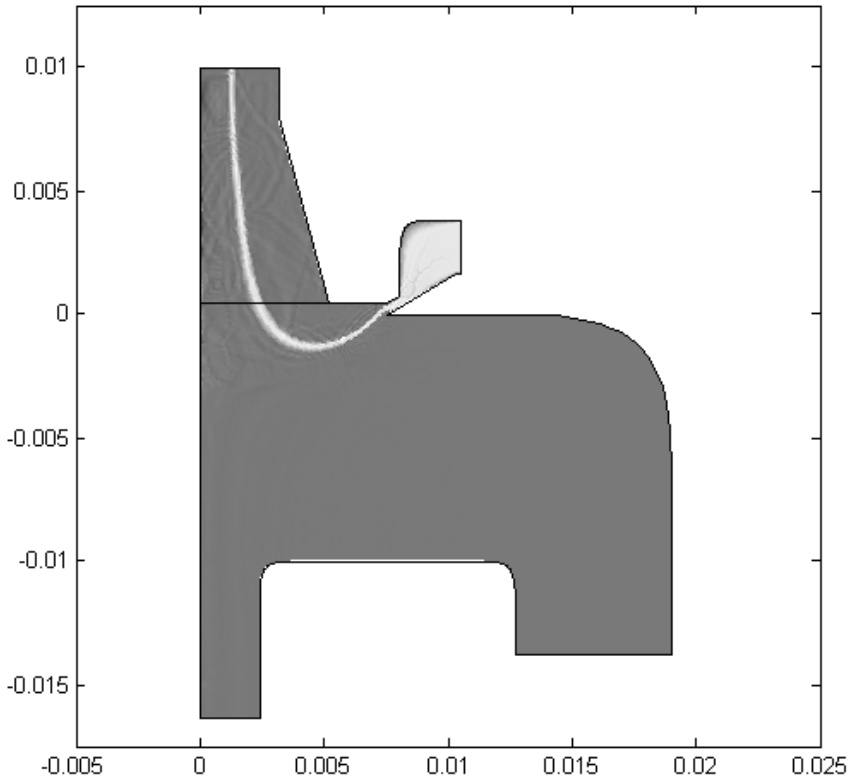

Figure 3.7. Electrokinetic Flow Solution without Mesh.

Solution to electrokinetic flow module for standard nano-RDMA geometry without the mesh on the excess outlet for 10 nm particles. The voltage was the ideal theoretical voltage necessary to transmit 10 nm particles.

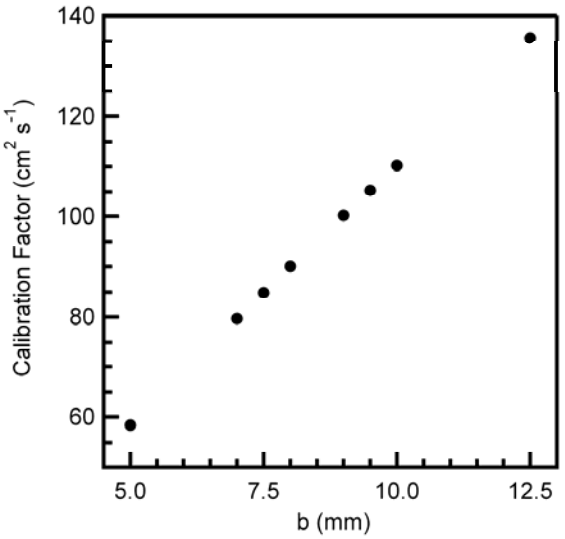

Figure 3.8. Calibration Factor for Electrode Spacing.

Calibration factor for different electrode gap spacings (*b*). The standard gap was 10 mm.

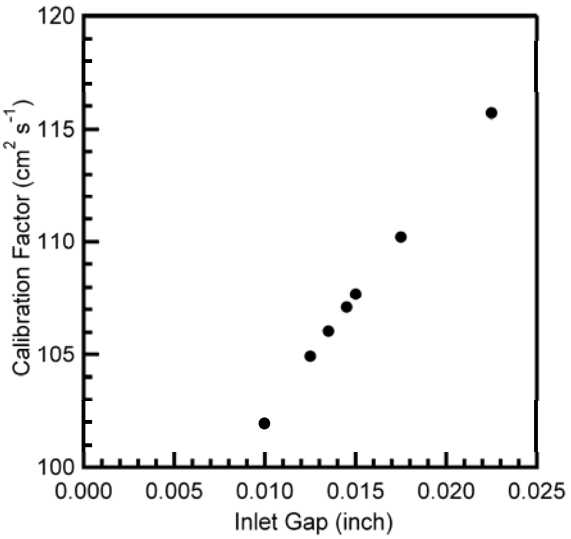

Figure 3.9. Calibration Factor for Aerosol Inlet Gap.

Calibration factor for different aerosol inlet gaps. The standard gap was 0.0175 inch.

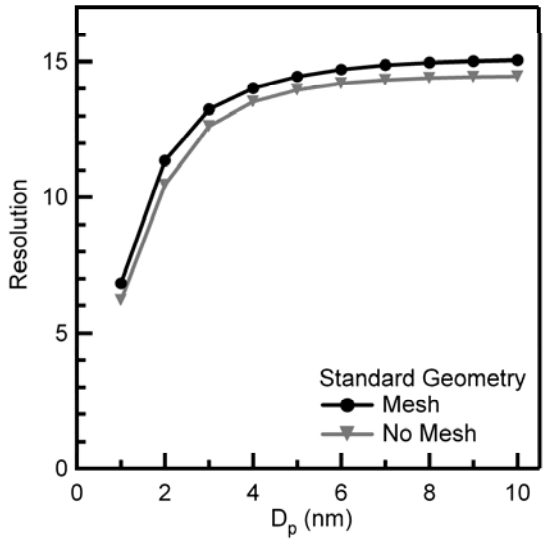

Figure 3.10. Resolution of nano-RDMA.

Comparison of the resolution for the standard nano-RDMA geometry with and without the mesh.

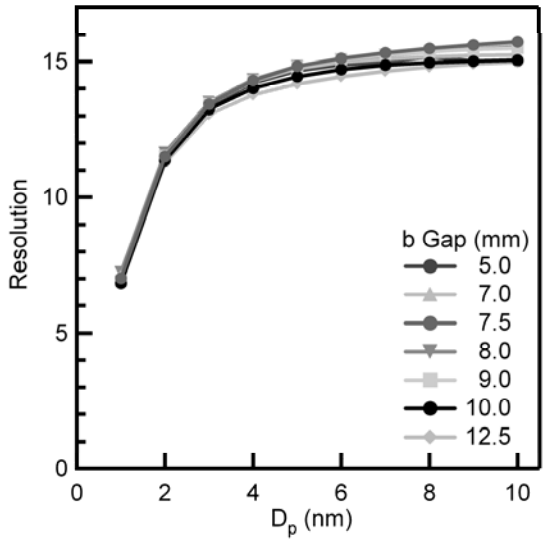

Figure 3.11. Resolution for Different Electrode Spacings.

Comparison of the resolution for the standard nano-RDMA geometry with different electrode gap spacings (*b*). The standard gap was 10 mm.

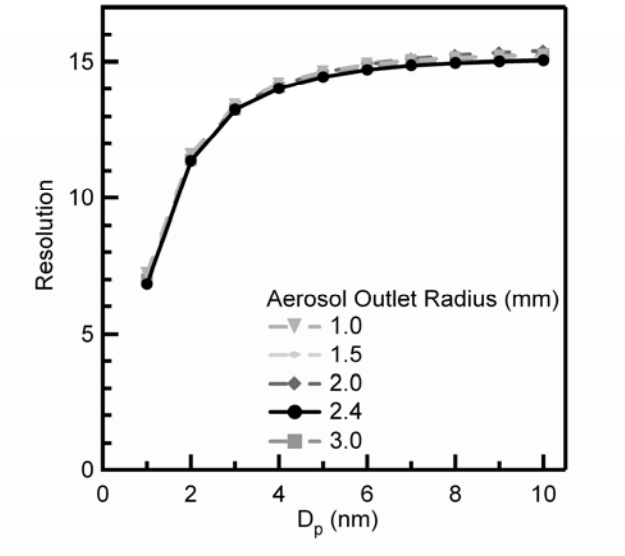

Figure 3.12. Resolution for Different Aerosol Outlet Gaps.

Comparison of the resolution for the standard nano-RDMA geometry for different aerosol outlet gaps (R_2). The standard gap was 2.4 mm.

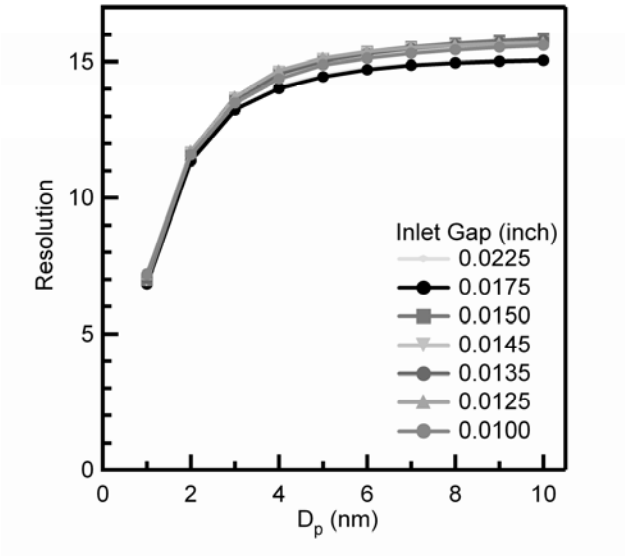

Figure 3.13. Resolution for Different Aerosol Inlet Gaps.

Comparison of the resolution for the standard nano-RDMA geometry with different aerosol inlet gaps. The standard gap was 0.0175 inch.

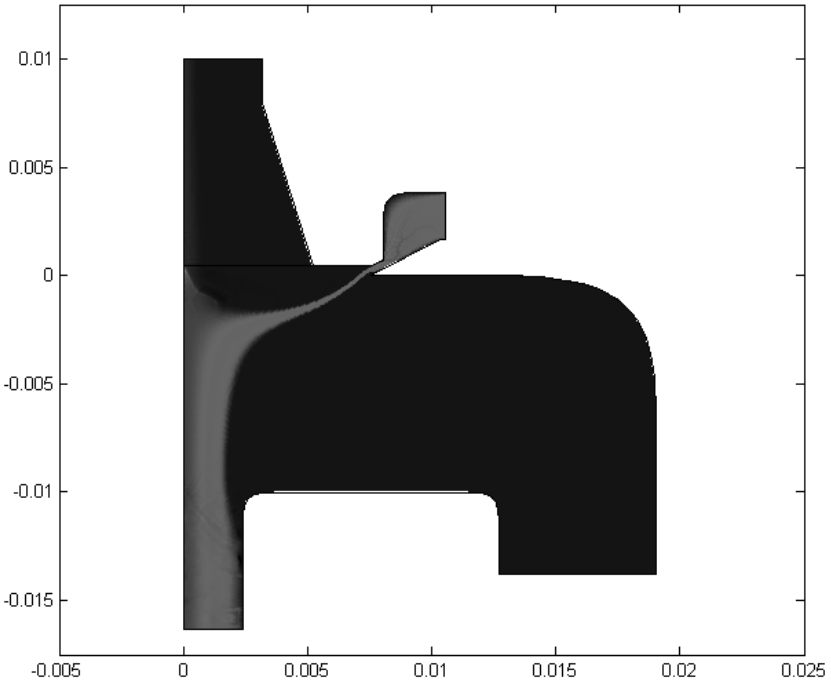

Figure 3.14. Electrokinetic Flow Solution at Optimal Voltage.

Solution to electrokinetic flow module for optimal voltage using the standard nano-RDMA geometry. The particle mobility diameter was 10 nm.

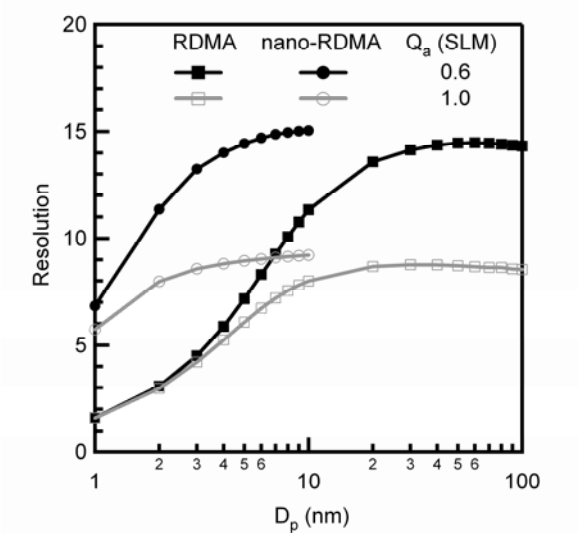

Figure 3.15. Resolution Comparison Between the nano-RDMA and RDMA.

Comparison of the resolution between the nano-RDMA and the RDMA using two different flow-rate ratios.

References

1. M. Kulmala, I. Riipinen, M. Sipila, H. Manninen, T. Petaja, H. Junninen, M. Maso, G. Mordas, A. Mirme, and M. Vana, *Science,* **318**, 89, 2007.
2. D. Holunga, R. Flagan, and H. Atwater, *Industrial and Engineering Chemistry Research,* **44**, 6332, 2005.
3. D. Rader, and P. McMurry, *Journal of Aerosol Science,* **17**, 771, 1986.
4. S. Friedlander, and D. Pui, *Journal of Nanoparticle Research,* **6**, 313, 2004.
5. J. Santos, E. Hontañón, E. Ramiro, and M. Alonso, *Atmospheric Chemistry and Physics,* **9**, 2419, 2009.
6. J. Rosell-Llompart, I. Loscertales, D. Bingham, and J. Fernandez de La Mora, *Journal of Aerosol Science,* **27**, 695, 1996.
7. D. Chen, D. Pui, D. Hummes, H. Fissan, F. Quant, and G. Sem, *Journal of Aerosol Science,* **29**, 497, 1998.
8. R. Flagan, *Aerosol Science and Technology,* **30**, 556, 1999.
9. N. Brunelli, R. Flagan, and K. Giapis, *Aerosol Science and Technology,* **43**, 53, 2009.
10. D. Chen, D. Pui, G. Mulholland, and M. Fernandez, *Journal of Aerosol Science,* **30**, 983, 1999.
11. D. Chen, and D. Pui, *Journal of Aerosol Science,* **28**, 985, 1997.
12. S. Zhang, Y. Akutsu, L. Russell, R. Flagan, and J. Seinfeld, *Aerosol Science and Technology,* **23**, 357, 1995.

13. *The script file had to be modified slightly for the simulations of the aerosol outlet radius. Decreasing the size of the outlet radius resulted in a re-numbering of the boundaries that required altering the boundary conditions appropriately.*

14. J. Fernandez de la Mora, *Journal of Aerosol Science,* **33**, 411, 2002.